Biomicrofluidics

Evaluation of 3D-printed molds for fabrication of non-planar microchannels

Cite as: Biomicrofluidics **15**, 024111 (2021); https://doi.org/10.1063/5.0047497
Submitted: 14 February 2021 . Accepted: 26 March 2021 . Published Online: 19 April 2021

Pravien Parthiban, Sindhu Vijayan, Patrick S. Doyle, and Michinao Hashimoto

Biomicrofluidics ARTICLE scitation.org/journal/bmf

Evaluation of 3D-printed molds for fabrication of non-planar microchannels

Cite as: Biomicrofluidics **15**, 024111 (2021); doi: 10.1063/5.0047497
Submitted: 14 February 2021 · Accepted: 26 March 2021 ·
Published Online: 19 April 2021

Pravien Parthiban,[1,2] Sindhu Vijayan,[1,3] Patrick S. Doyle,[2] and Michinao Hashimoto[1,3,a)]

AFFILIATIONS

[1]Pillar of Engineering Product Development, Singapore University of Technology and Design, 8 Somapah Road, Singapore 487372
[2]Department of Chemical Engineering, Massachusetts Institute of Technology, 77 Massachusetts Ave., Cambridge, Massachusetts 02139, USA
[3]Digital Manufacturing and Design Centre, Singapore University of Technology and Design, 8 Somapah Road, Singapore 487372, Singapore

[a)]**Author to whom correspondence should be addressed:** hashimoto@sutd.edu.sg

ABSTRACT

Replica obtained from micromolds patterned by simple photolithography has features with uniform heights, and attainable microchannels are thus quasi-two-dimensional. Recent progress in three-dimensional (3D) printing has enabled facile desktop fabrication of molds to replicate microchannels with varying heights. We investigated the replica obtained from four common techniques of 3D printing—fused deposition modeling, selective laser sintering, photo-polymer inkjet printing (PJ), and stereolithography (SL)—for the suitability to form microchannels in terms of the surface roughness inherent to the mechanism of 3D printing. There have been limited quantitative studies that focused on the surface roughness of a 3D-printed mold with different methods of 3D printing. We discussed that the surface roughness of the molds affected (1) transparency of the replica and (2) delamination pressure of poly(dimethylsiloxane) replica bonded to flat glass substrates. Thereafter, we quantified the accuracy of replication from 3D-printed molds by comparing the dimensions of the replicated parts to the designed dimensions and tested the ability to fabricate closely spaced microchannels. This study suggested that molds printed by PJ and SL printers were suitable for replica molding to fabricate microchannels with varying heights. The insight from this study shall be useful to fabricate 3D microchannels with controlled 3D patterns of flows guided by the geometry of the microchannels.

INTRODUCTION

This paper discusses the suitability of poly(dimethylsiloxane) (PDMS) replicas from four different three-dimensional (3D) printing methods for the fabrication of microchannels with dimensional fidelity. We evaluated four consumer 3D printers and PDMS replica for their abilities (1) to create smooth surfaces applicable for replica molding and oxidative sealing of PDMS to glass, (2) to create microchannels with varying heights along and across the direction of the flow, and (3) to fabricate microfluidic channels that are closely spaced in position. Microfluidics has found applications in a diverse array of fields such as chemical and biological analytics, medical diagnostics, chemical and material synthesis, drug discovery, controlled heat transfer, and biotechnology.[1–12] A key breakthrough in technology that heralded the rapid spread of microfluidics is soft lithography. Soft lithography involves the use of molds (alternatively called masters) typically patterned by photolithography to replicate microchannels in poly(dimethylsiloxane) (PDMS).[13] The enduring popularity of soft lithography is down due to certain inherent advantages; soft lithography is a simple, safe, low-cost, and rapid process to prototype PDMS microchannels. PDMS is an optically clear, biocompatible material that can be reversibly or irreversibly bonded to different substrates.[14,15] Furthermore, the permeability of PDMS to gases is critical to applications in microfluidics,[16,17] and its elastomeric nature has been exploited in the engineering of valves and other elements to control fluids.[18–20] Recent development of custom-made materials has enabled photocurable PDMS possessing properties similar to Sylgard 184 to be directly printed via stereolithography (SL) 3D printing.[21] Despite such advanced demonstration, however, heat-curable and castable PDMS resins (such as Sylgard 184) have been widely used for the replication of micropatterns.

Replica molding and soft lithography remain arguably one of the most popular techniques for the fabrication of microchannels, especially in academic settings for research. Conventional soft lithography using cleanroom facilities mostly produces planar, two-dimensional (2D) microchannels. Herein, we define planar, 2D microchannels as those having uniform height and rectangular cross sections. We define non-planar, 3D microchannels as those that have cross-sectional shapes other than rectangles and those that have varying heights. A single-step photolithography results in replica with planar molds where all features have the same height. Such planar geometries restrict the choice of fluids to be used, and additional surface modification is often required to change the wettability of channels.[22,23] The fabrication of molds for microchannels with arbitrary cross sections or varying heights by photolithography requires a multi-step process that involves the manual alignment of multiple masks.[24,25] Some examples of replicated 3D microchannels have demonstrated the potential to use flows in 3D spaces. Mixing at a low Reynolds number can be enhanced by the integration of grooves on the surface of microchannels.[26] Stepped or terraced microchannels have been used in the robust, high throughput generation of droplets.[27,28] Gradients in confinement have been exploited to generate and manipulate droplets in a facile manner.[29–31] Furthermore, 3D microchannels have been used to manipulate cells.[32,33] Despite these successes, fabricating non-planar, 3D microchannels by conventional soft lithography demands intensive labor and time as it requires the fabrication of multiple masks with separate alignment and exposure for each. Due to this limitation, the majority of PDMS microchannels fabricated using conventional soft lithography have rectangular cross sections, and they are quasi-2D in nature without variations in height. As such, there is much current interest in developing facile methods to fabricate molds for 3D microchannels.

3D printing has emerged as a promising candidate to fabricate 3D microchannels. 3D microchannels can easily manipulate multiphase flows and help form templates with different spatial arrangements.[34] In 3D printing, a computer-aided design (CAD) model of a 3D object, decomposed into a sequence of 2D slices is used to fabricate the physical object in a layer-by-layer fashion. The process is automated, and it is suitable for the fabrication of arbitrary 3D structures. 3D printing majorly contributes to microfluidics through the fabrication of molds for replication,[35–45] entire devices,[46–48] connectors/subunits for microfluidic devices,[49–52] and partial units that can be integrated to form microchannels.[53] Among the different ways, 3D printing of molds for replication is derived from the conventional soft lithography where a master mold is used to replicate microchannels. 3D printing of entire devices provides a fast route to produce microfluidic chips. However, evacuation of uncured resin[52,54] from narrow channels and removal of sacrificial support materials[50] remains a challenge. Besides, SL printing of entire microchannels may suffer from unintended photopolymerization of the channel region from the subsequent illumination, which has been partially addressed by adding photoabsorbers to the resins. To circumvent the issues of clogging of material, researchers have adopted the fabrication of modular and partial units that can be post-assembled to form microfluidic devices. To this end, 3D printing of molds serves as a facile and general approach for the replication of PDMS microchannels.[35–45] Currently, there is no consensus on the best 3D printing technique for fabricating molds for replicating PDMS microchannels, especially with regard to fabricating molds for 3D microchannels. Given that there are many readily available consumer 3D printers in the market, there is a need for the careful evaluation of 3D printers for their suitability to fabricate molds harboring microfeatures. While there are a few investigations into the suitability of 3D printers to fabricate an entire microchannel,[55–58] cross-platform studies to evaluate 3D printing of soft lithography molds remain lacking.[59] In particular, there are limited quantitative studies that focused on the surface roughness of 3D-printed mold fabricated with different methods of 3D printing and the resultant bonding strength of PDMS replica with planar substrates. Furthermore, the feasibility to replicate planar and non-planar microchannels and closely packed microchannels with dimensional fidelity is worth investigating.

In this paper, we evaluated PDMS replica from four common methods of 3D printing to contain non-planar microchannels and closely packed microchannels. The replica used for the evaluation were obtained from four methods of 3D printing such as fused deposition modeling (FDM), selective laser sintering (SLS), photopolymer inkjet printing (PJ), and stereolithography (SL). All these printers were used to fabricate monolithic master molds to replicate PDMS microchannels. The microstructures of the master molds (with varying heights and cross sections) were fabricated in an automated and single attempt of 3D printing, followed by post-processing. We quantified the surface roughness of the molds and the delamination pressure of the microchannels sealed with the glass substrates. The impact of surface roughness of the mold on the transparency of PDMS replica was also analyzed. Based on these measurements, we filtered the printers that are suitable for fabricating molds for microfluidic devices. The replica from these suitable printers was then tested for their accuracy to transfer the designed dimensions and cross-sectional shapes from the molds. The study described in this paper should provide useful guidelines to fabricate 3D microchannels using 3D printing and replica molding, which would allow designing 3D flows in microchannels for various applications.

RESULTS AND DISCUSSION

Research aim and approach

The aim of our study was to evaluate PDMS replica of planar and non-planar channels obtained from molds printed by different types of 3D printers. Our evaluation included two steps—(1) examination of surface roughness and bonding strength and (2) testing the accuracy in dimensions of replicated microchannels. In the first step, the four molds from different printing mechanisms and their PDMS replica were examined for their surface roughness (i.e., arithmetic mean roughness, R_a) and bonding strength correspondingly. The measure of surface roughness and the resulting delamination pressure were used to screen the printers not suitable for the fabrication of molds. Subsequently, we tested the accuracy of printed dimensions in the replicas from the selected printers. The dimensions of the printed channels (i.e., width and height) were measured and compared against the designed dimensions. The data were analyzed in the form of deviation and error percentage, with the mean and standard deviations.[60–62]

Surface roughness of the printed molds

Molds used for soft lithography must satisfy three essential criteria. First, the molds used should be physically robust. The submillimeter features should not be destroyed by the repeated casting of PDMS. Second, the molds should not chemically interfere with the curing and removal of PDMS. Finally, the surfaces of the replicated PDMS structures should be smooth enough to allow facile bonding with substrates. In our experiments, the molds printed by QiDi Tech 1 (FDM) and EOS Formiga (SLS) 3D printers were used as printed, while the molds printed by Objet30 Prime (PJ) and Structo OrthoForm (SL) printers required washing and processing as described in Materials and methods section. The photographs of molds printed by these printers are shown in Fig. S1 in the supplementary material.

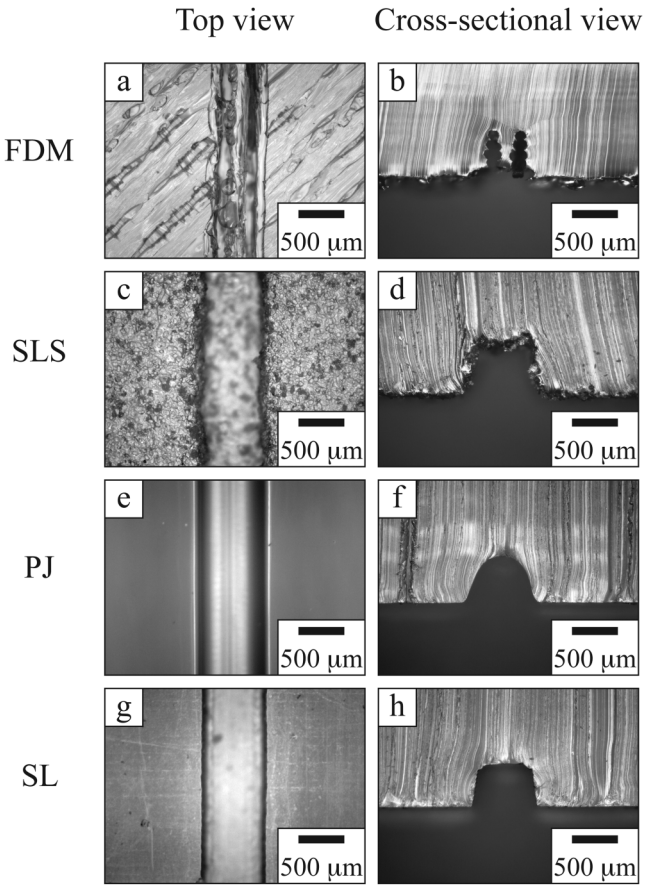

FIG. 1. Photomicrographs of PDMS microstructures ($w_D = 500\,\mu$m, $h_D = 500\,\mu$m) replicated from molds fabricated in four different techniques of 3D printing. (a) and (b) Fused deposition modeling (FDM), (c) and (d) selective laser sintering (SLS), (e) and (f) photo-polymer inkjet printing (PJ), (g) and (h) stereolithography (SL). (a), (c), (e), and (g) Photomicrographs showing the top view of microstructures replicated in PDMS. (b), (d), (f), and (h) Photomicrographs showing the cross-sectional view of the microstructures replicated in PDMS.

We found that molds printed using QiDi Tech 1 (FDM) and EOS Formiga (SLS) printers were relatively rough and the microstructures replicated in PDMS using these molds also retained rough surfaces. The photomicrographs of the top and cross-sectional view of PDMS replica by the four printing methods visually depict the roughness of the molds (Fig. 1). R_a values (defined as arithmetical average roughness) of the four 3D-printed molds of FDM, SLS, PJ, and SL are measured to be 16.7 (SD = 2.6), 3.3 (SD = 0.3), 2.3 (SD = 0.4), and 1.4 μm (SD = 0.4 μm), respectively. This roughness affected conformal contact of replicated PDMS with glass substrates and thus inhibited chemical bonding via plasma oxidation. The surface profiles of the four 3D-printed molds and the top view of PDMS microchannels are given (Fig. 2). The surface roughness of PDMS replica was due to the surface roughness of the mold, which was inherent to the mechanism of printing. The rough surfaces of PDMS replica compromised the optical transparency, which is an important requirement for the PDMS devices.

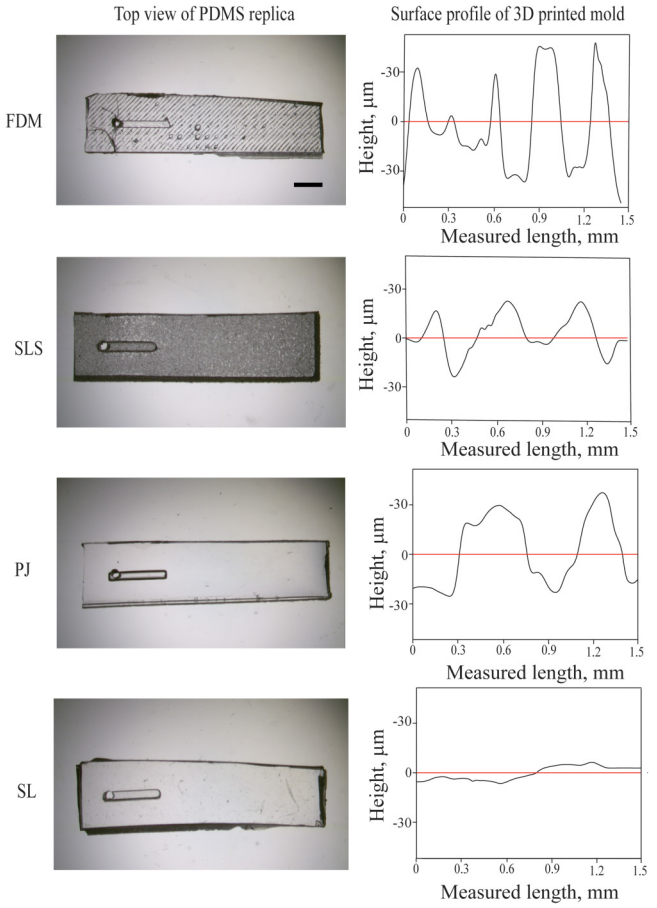

FIG. 2. Photomicrographs of PDMS replica and plot showing the surface profile of the four 3D-printed molds—fused deposition modeling (FDM), selective laser sintering (SLS), photo-polymer inkjet printing (PJ), and stereolithography (SL).

PDMS casting/bonding

Molds fabricated by FDM and SLS printers were made of solid materials (e.g., filaments and particles), and PDMS was directly cast without any post-processing. PJ and SL printing are based on the polymerization of photocurable liquid resins; it has been reported that the presence of the photoinitiators can interfere with the polymerization of PDMS precursors cast on the molds printed by SL and PJ.[63] Removal of remaining photoinitiators and unpolymerized monomers after 3D printing was, therefore, essential for the successful replication. Heating, exposure to ultraviolet (UV) light, and washing with solvents are suggested by the manufacturers as post-processing. Alternatively, the surface of the mold can be rendered passive by coating it with an inert material.[33,34,40,41] The post-processing used to treat the molds used in this study is described in Materials and methods section. The PDMS replica obtained from the molds of four different printers (FDM, SLS, PJ, and SL) was then bonded to glass by plasma oxidation. Ideally, the molds should be used in a similar way to those fabricated with SU-8 and a silicon wafer to maintain the convenience of soft lithography. We, therefore, did not explore other methods of bonding such as the use of partially cured PDMS as a sealant for our microchannels. The layer of partially cured PDMS might give rise to an additional height of the channels and also it can clog the narrow channels.

Bonding strength of PDMS replica

The bonding strength of the replica obtained from each method of 3D printing was confirmed by measuring the delamination pressure. The replica from FDM-printed mold did not covalently bond to the glass after plasma oxidation. The replica was readily detached from glass due to its surface roughness. Therefore, sealed PDMS channels (width × height × length = 900 μm × 900 μm × 1 cm) obtained from the other three printers (SLS, PJ, and SL) were taken for the testing. Colored water was pumped into the channels using a pressure-driven fluid dispenser. The applied pressure was 50 kPa and was increased in the increments of 25 kPa. PDMS replica obtained from the mold printed by SLS printer failed at 50 kPa (characterized by delamination from the glass). At 150 kPa, PDMS replica obtained from PJ printer started to leak from a single point. This leakage occurred from a gap along a straight line (due to a positive feature of the mold). Such a linear gap may occur in the direction parallel to the movement of the nozzle of PJ printer. PDMS replica from SL printer held the internal pressure up to 400 kPa; the leakage happened at 400 kPa at the interface between the tubing and PDMS. It has been reported that a PDMS replica obtained from silicon molds sealed to glass by plasma oxidation withheld the pressure in the range between 206 and 345 kPa.[14] Our measurements suggested that the molds obtained from PJ and SL printing allowed fabricating microchannels that handled pressures up to 125 and 375 kPa, respectively, which would be sufficient to use the devices for representative microfluidic experiments.

These observations on the surface quality and bonding of PDMS replica suggested that the molds printed using FDM and SLS printers were not suitable for replica molding. A high surface roughness resulted in poor bonding and delamination from the glass and a non-transparent surface impairing visualization. Replica from FDM-printed mold did not bond to the glass substrate owing to the surface roughness created by imprints of the printed layers. These layer imprints are influenced by the nozzle diameter of FDM 3D printers. A commonly used nozzle is with a diameter of 400 μm. PDMS replica produced from SLS-printed molds were bonded to glass but the grainy texture on the surface affected transparency. The applicability of SLS printing for the fabrication of micromolds was also hampered by the difficulty to remove unsintered particles from small cavities[64] and the grainy surface finish.[65] The grains on the surface of SLS-printed mold also tended to adhere to PDMS replica during the replication. For SLS printers, the use of small particles would, in principle, reduce the surface roughness, but such printers are not widely available at this time; the sizes of particles of representative SLS printers are >50 μm (Table S1 in the supplementary material). The use of fine particles for SLS printing is also reported to cause coagulation of particles, which were not suitable for the current application.[66] Post-processing of FDM and SLS-printed parts was generally carried out by mechanical (e.g., eroding, milling) and chemical (e.g., coating, dissolution) treatments.[67–71] Despite these successful demonstrations, however, we did not explore those options in this study because such treatments might alter the shape and dimensions of microscale features. The current study focused on the capability to use 3D micromolds for the fabrication of microchannels without such treatments.

Accuracy of 3D printing:Planar microchannels

We identified PJ and SL as suitable mechanisms of 3D printing to fabricate molds for microchannels. We further tested the accuracy of printing by measuring the dimensions of features printed by Objet30 Prime (PJ) and Structo OrthoForm (SL) 3D printers. PJ and SL printers operate in different mechanisms. 3D-printed models by PJ printer are influenced by the size of resin droplets, space between the droplets, and spreading of resin, while 3D-printed models by a SL printer depend on the size of a pixel and curing time. Therefore, the same design input is expected to generate different microstructures. To test the accuracy of dimensions by these printers, we printed a 5 × 5 array of cuboid microstructures. The microstructures were designed to have widths, w_D = 0.1, 0.3, 0.5, 0.7, and 0.9 mm and heights h_D = 0.1, 0.3, 0.5, 0.7, and 0.9 mm. We defined w_D and h_D as the widths and heights designed in CAD, respectively. Both Objet30 Prime (PJ) and Structo OrthoForm (SL) fabricated structures as small as h_D = 0.1 mm (which was the smallest height we tested). This height is more than the layer thickness of the printers. Structo OrthoForm (SL) was not able to print structures with w_D = 0.1 mm [resolution $(x \times y) = 0.1 \times 0.1$ mm^2] and the minimum printable width was 0.3 mm. While Objet30 Prime (PJ) was able to print structures with w_D = 0.1 mm [resolution $(x \times y) = 0.042 \times 0.042$ mm^2], the printed heights for these structures were less than the designed heights. PDMS was cast on the microstructures, and cross sections of the replicated microstructures were imaged under a low magnification inspection microscope. In this paper, we used PDMS replica to measure the dimensions of the channels. The use of PDMS stamps allowed slicing the channels to visualize the cross-sectional profile. We note that PDMS replica generally expands laterally (i.e., x, y-directions) after the release from the mold due to its high

thermal expansion coefficient (300×10^{-6} 1/K),[72,73] which would affect the dimension of the channels. The expansion was not prominent in the current study, and we used PDMS replica to study the dimensions of the channels. The maximum widths (w_M) and maximum heights (h_M) of the replicated microstructures were measured from the cross sections [Figs. 3(a) and 3(b)]. The datapoints of w_M were obtained by averaging the measured width over the range of design height ($h_D = 0.1$, 0.3, 0.5, 0.7, and 0.9 mm) [Fig. 3(c)]. Similarly, the data points of h_M were obtained by taking the average of measured height over the range of design width ($w_D = 0.3$, 0.5, 0.7, and 0.9 mm) [Fig. 3(d)]. These plots show the systematic deviation between the design and printed dimensions of the channel. The absolute percent error for the width and height for a replica from SL-printed mold is calculated to be in the range of 7%–20% and 2%–8% respectively. Similarly, the percent error for a replica from PJ-printed mold is 31%–125% and 2%–7% for the width and height, respectively.

This increase in the width of PDMS replica can be attributed to the mechanism of printing employed by PJ printers. In PJ printers, there is a time-lapse between the resin deposition by the printer head and curing of the deposited resin by the UV lamp. The time lag between deposition and curing allowed the resin to reflow and spread.[55,56,74] The spreading of resin on the build tray resulted in the widening of the width. This shows a large deviation between the designed and the printed widths of PJ printers [Fig. 3(c)]. SL printers do not have a limitation concerning the spreading of resin; the walls of SL-printed molds are relatively straight (compared to PJ-printed molds); the slanted vertical walls are due to the diffraction of the light illuminated to the photoresin. For printers with similar specifications in lateral (x, y) resolutions, SL printers should have better accuracy for printing than a PJ printer in the lateral dimensions of printed structures.

Our characterizations demonstrated the printability of straight channels using PJ and SL printers. It is worth mentioning that these two printers are also capable of fabricating curved channels (such as arcs and serpentine shapes). The minimum pixel dimensions of SL and PJ printers used in this study were 50 and 42 μm; the lateral dimensions of the printed features were increased by ~100 and ~250 μm for the same SL and PJ printers [Fig. 3(c)]. Both SL and PJ printers are based on liquid resins, and the surface tension of the liquid resin would promote the formation of continuous smooth edges rather than pixelated edges along the defined curvature. The minimum curvature that can be printed would depend on multiple factors including the type of resin, the printed layer height, and the minimum pixel size, which is left for further investigation.

Accuracy of 3D printing: Non-planar microchannels

The design of a microfluidic device includes channels of varying dimensions and geometries (straight and curved features). In our work, we assessed the replica from suitable printers (PJ and SL) for its ability to form both rectangular and non-rectangular geometries. Various non-rectangular geometries comprising gradients in height, curves, and slanted lines were designed, printed, and replicated in PDMS to assess 3D printers. Microstructures with slopes varying from 1.4° to 21.8° were fabricated using Objet30 Prime (PJ) and Structo OrthoForm (SL). Subsequently, the printed structures were replicated in PDMS. The cross sections of PDMS replicas were observed under a microscope. We observed that the height of channels increased in discrete steps [Figs. 4(a) and 4(b)].

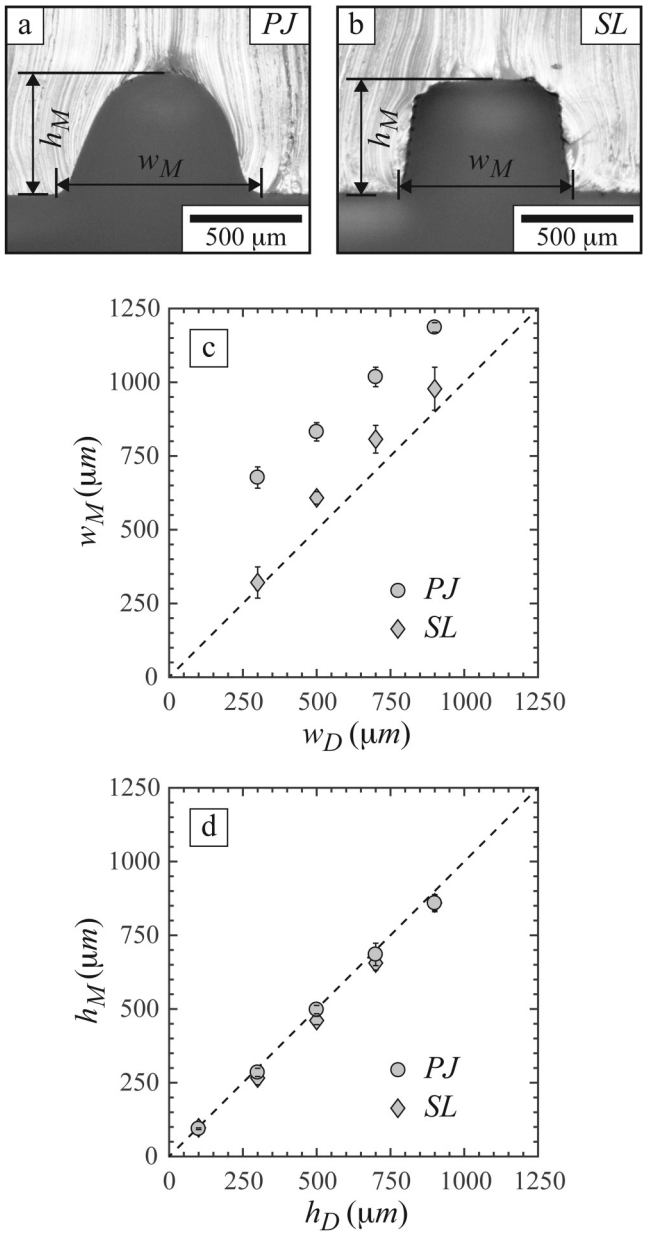

FIG. 3. (a, b) Cross-sectional view of PDMS microstructures replicated from molds that were printed using Objet30 Prime (PJ) and Structo OrthoForm (SL). The photomicrographs show representative measurements of maximum width (w_M) and height (h_M). (c) The plot of the measured maximum width (w_M) of PDMS microstructures against the designed width (w_D). (d) The plot of the measured maximum height (h_M) of PDMS microstructures against the designed height (h_D).

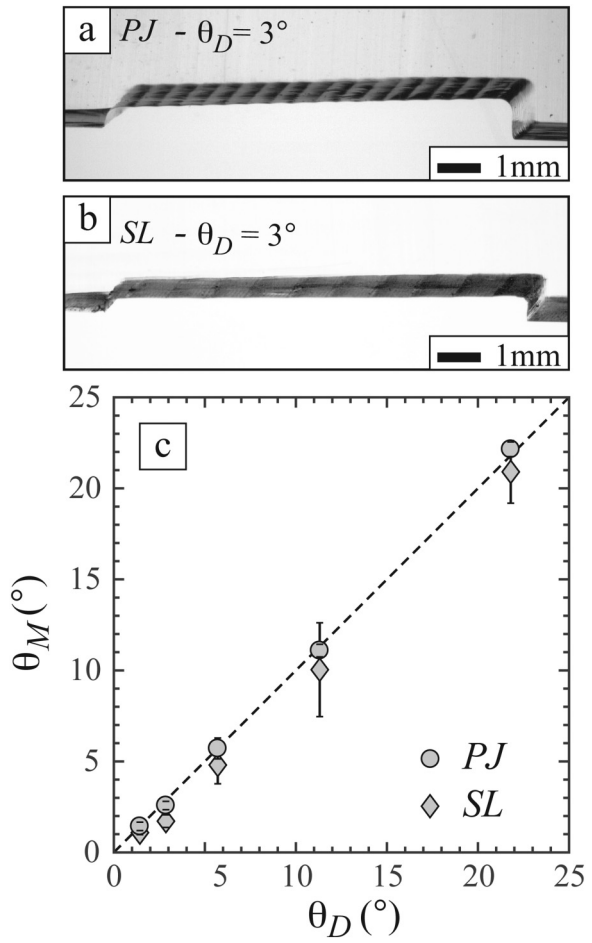

FIG. 4. (a) Stereomicroscopic images of sloped PDMS structures replicated using Objet30 Prime (PJ). (b) Stereomicroscopic images of sloped PDMS structures replicated using Structo OrthoForm (SL). The samples were slightly tilted away from a nominal side-view to give a 3D view. The discrete increase in heights was evident in the photomicrographs. (c) The measured slope of the microstructures, θ_M, plotted against the designed slope, θ_D.

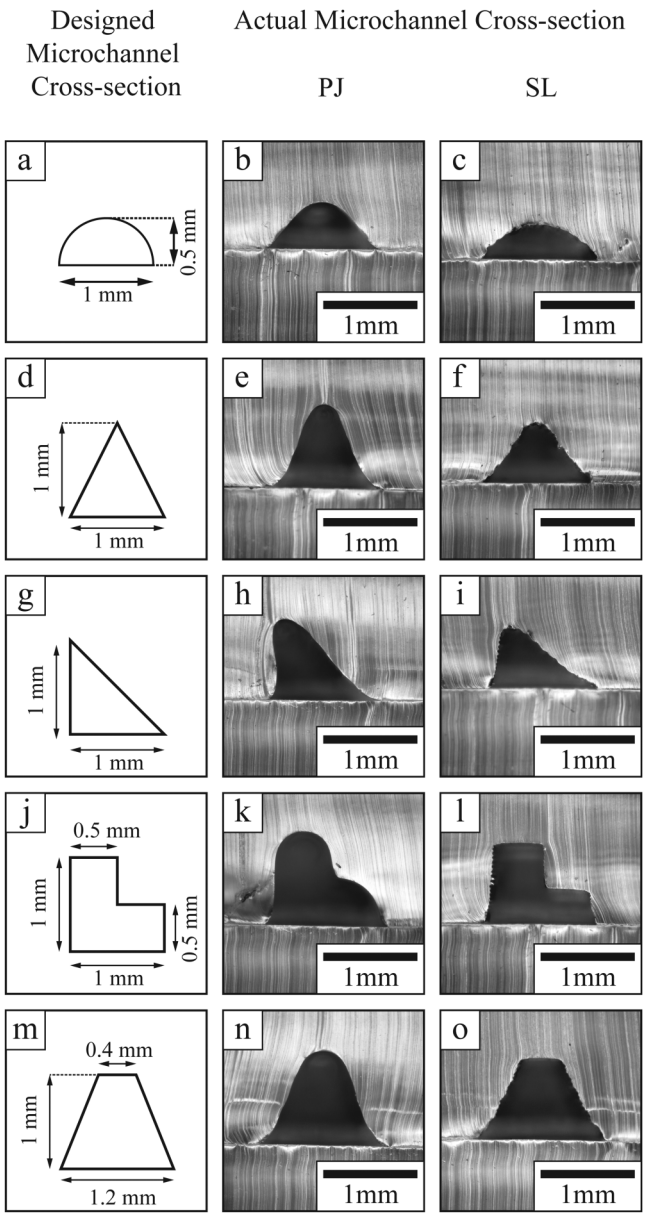

FIG. 5. (a), (d), (g), (j), and (m) Design of microchannels of non-rectangular cross sections. (b), (e), (h), (k), and (n) Photomicrographs of the cross section of PDMS microchannels replicated from molds printed using Objet30 Prime (PJ). (c), (f), (i), (l), and (o) Photomicrographs of the cross section of PDMS microchannels replicated from molds printed using Structo OrthoForm (SL).

Objet30 Prime (PJ) prints with a smaller layer height (28 μm) than Structo OrthoForm (SL) which prints with a layer height of 50 μm. The microstructures replicated from molds printed with Objet30 Prime had a relatively smooth increase in height. A smaller lateral (x, y) resolution and vertical (z) resolution allows Objet30 Prime (PJ) to print sloped structures with better accuracy than Structo OrthoForm (SL) [Fig. 4(c)].

It is also essential that 3D printers accurately reproduce the design of the cross sections of microchannels. We qualitatively studied the ability of these 3D printers to fabricate various shapes of cross sections of the channels: semi-circular, triangular, trapezoidal, and stepped patterns. The microchannels were replicated in PDMS. Photomicrographs of the cross sections of the microchannels and the sketches of their original design are shown (Fig. 5). Our experiments suggested that the molds for microchannels with flat top surfaces, and straight sidewalls were printed and replicated more accurately by SL printer than PJ printer. Microstructures with semi-circular and triangular shapes were not reproduced by either printer. The lateral resolutions of the used printers were greater than 100 μm. As a

result, these printers could not accurately fabricate the parts of the CAD model with the lateral dimension approaching zero (e.g., a vertex of a triangle). Despite the difference in the layer height for the two printers, these differences can also be attributed to the mechanism of printing. The smooth transition between the slopes and the increase in the width of the structures printed by PJ printers are due to the reflow and spreading of resin. This reflow of resin can be visualized by the curved regions at the corners increased width of the features. Such changes affect the accuracy of the cross-sectional shape of the replicated features acquired from the mold printed in PJ printers. While in SL printer, the layers are projected as discrete entities into the resin vat and the structures are formed over the build plate. Since the resin is confined in a bath, there is no scope for the spreading of the resin. Furthermore, the surface of the resin in the bath remains flat. The shapes of microstructure replicated from SL-printed mold, therefore, conformed relatively close to the design, with vertical sidewalls and a flat top wall.

Fabrication of closely spaced microchannels

Many microfluidic applications require devices with a small footprint. Herein, the ability to fabricate microfluidic devices with minimal spacing between adjacent microchannels is crucial. To test this capability, a microfluidic device with nine parallel microchannels with identical square cross sections was designed and printed ($w_d = h_d = a$). The spacing between adjacent microchannels (δ) was varied from 1400 to 100 μm [Fig. 6(a)]. Five of such microfluidic devices were replicated from the molds, each having the same variation in the inter-channel spacing but with microchannels of different sizes (a = 300, 500, 1000, 1500, and 2000 μm). Water with a blue food dye was passed through the microchannels and observed under a microscope to check for any cross-flow between adjacent microchannels. The spacing was measured as the distance between the edges of the adjacent microchannels. The smallest inter-channel spacing required was determined as the one where there was no cross-flow between adjacent microchannels throughout the length. The minimum spacings were measured as discrete data based on the design dimensions of the gaps. For the microchannels fabricated from 3D-printed molds using Objet30 Prime (PJ), the minimum spacing required between two adjacent microchannels was 600 μm [Fig. 6(b)]. For the microchannels fabricated from 3D-printed molds using Structo OrthoForm (SL), the minimum spacing required between two adjacent microchannels varied from 600 to 800 μm. The minimum distance required between adjacent microchannels for the varying microchannel sizes (a) is plotted [Fig. 6(c)]. With both 3D printers, the minimum required spacing was greater than the smallest channel width that can be printed.

In PJ printing, the spreading of the deposited resin can bridge the positive features defining the microchannels, which causes closely spaced microchannels to become connected. The spreading of resin in PJ printing is consistent, regardless of the width and height of the channels. Therefore, a constant gap (600 μm) was required for the mold fabricated by PJ printer. In SL printing, the light is illuminated only to the features defining the microchannels, and the resin in the gaps between the positive features should remain unpolymerized. In practice, however, we found that

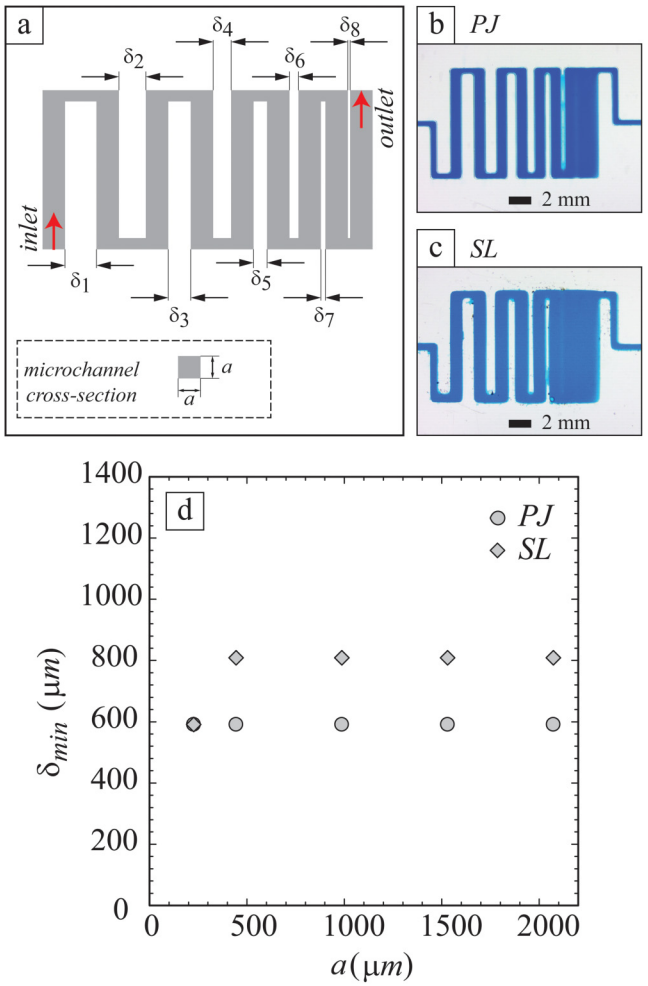

FIG. 6. (a) Schematic of the microfluidic device used to determine the minimum spacing required between adjacent microchannels. In a given microfluidic device, the inter-channel spacing (δ) was varied—δ_1 = 1400 μm, δ_2 = 1200 μm, δ_3 = 1000 μm, δ_4 = 800 μm, δ_5 = 600 μm, δ_6 = 400 μm, δ_7 = 200 μm, and δ_8 = 100 μm. (b) and (c) Photomicrographs of the microchannel with water (colored with a food dye) flowing through them. PDMS microchannels were replicated from molds 3D-printed using (b) photopolymer inkjet printing (PJ) and (c) stereolithography (SL). (d) The minimum inter-microchannel spacing required to avoid crossflow between neighboring channels, plotted for microchannels of different nominal sizes.

overexposure of the resin in the gaps (i.e., the spaces between two structures) can cause unintended polymerization,[75,76] which resulted in the bridge between two adjacent microchannels. This consideration was consistent with our observation that the adjacent channels were likely to be merged when the channels were high; the higher number of exposures was required to create the larger relief structures on the mold, and consequently, the gaps were likely to be filled by overexposure. The bridging of the gaps in SL printers is subjected to light irradiation, time of exposure, and

reactivity of the resin. These parameters vary from printer to printer. One of the plausible ways to limit this bridging between microchannels in SL printing is by adding appropriate photoabsorbers to minimize overexposure to the light. The use of resins with light-absorbing properties improves the resolution of SL printing.[52] However, our finding also suggested the print resolution of the positive features (257 μm) was greater than that of the negative features (600 μm), indicating the challenges to create multiple channels in proximity. In general, adequate characterization should be performed to fabricate the mold for closely packed microchannels using SL and PJ printers.

Printer specification and printing mechanism

Our experiments are based on a particular 3D printer of each type, and the outcomes of our study about the representative printers are influenced by both the specification of the chosen printer and the inherent printing mechanism. This paper aims to highlight the importance of the mechanisms of 3D printers for their performance to create molds suitable for microfluidics. Such considerations allow us to make an informed guess for the performance of each printer to create microfluidic molds.

For instance, factors specific to the printer include the size of the nozzle in FDM, size of particles in SLS, time-lapse between resin deposition and UV curing in PJ, curing time, and the reactivity of the materials in SL. By altering these factors, we can improve the surface quality of molds and the fidelity of replicated microchannels. However, the use of solid materials in FDM and SLS printers, spreading of resin in PJ, and unintended curing of the resin in SL are inevitable factors attributed to the mechanism of printing. Similarly, the layer height would affect the attainable width of the printed pattern. An increase in the layer height would result in an increase in the channel width in PJ printers due to resin spreading, while the effects would be minimal in SL printers. In terms of deviation between designed and printed features (both lateral and cross-sectional dimensions), we observed that SL printer produced less deviation from the design than PJ printer. This observation is in accordance with previous studies on these printers.[59] While PJ printers produced features that deviated largely from the designed features, it was reported that PJ printer is still suitable for the fabrication of molds for complex and intricate patterns such as small-angled structures, vias, thin membranes, and rounded channels.[37,77] The inherent semi-circular cross section of PJ-based mold can be advantageous for the fabrication of well-established components such as pneumatic valves. As for the post-processing of the mold, the removal of rubbery support of PJ-printed parts generally takes longer than the removal of residual resin from SL-printed parts. Alternative approaches such as fabricating open channels were employed for the ease of the removal of support from molds of PJ printer.[77]

In choosing one printing technique over the other, it is crucial to identify the factors affecting the quality of the replicated features. The surface quality of the molds and bonding strength of the channels can be improved by the use of industrial-grade printers. Nevertheless, our study also suggested that the feasibility to apply desktop SL printers to create microchannels via replica molding. While molded microfluidic devices are currently limited by the resolution of 3D printers (currently available consumer PJ and SL printers have a typical lateral resolution of 100 μm), emerging technologies allow printing at improved resolutions.[78,79] Most PJ printers remain as proprietary systems and the installation and maintenance cost of PJ printers remains rather high. Due to the availability of inexpensive projectors and laser sources, desktop SL printers may be suitable for academic laboratories and educational institutes.

CONCLUSIONS

In this paper, we evaluated the suitability of PDMS replica from four different 3D printing techniques for their fabrication of microfluidic devices and dimensional fidelity. We evaluated 3D printers and corresponding replica in two sequential steps. In the first step of evaluation on surface roughness, we found that replicated channels from molds printed using FDM and SLS printers exhibited rough and non-transparent surfaces that were not suitable for fabricating PDMS microchannels. In contrast, PDMS replica from molds of PJ and SL printers formed 3D microfluidic devices in a facile way and exhibited delamination strength comparable with PDMS replica fabricated using a silicon wafer patterned with SU-8. We also found that fabrication of closely spaced channels was challenging with 3D printers and materials we investigated; the minimum distances required to prevent merging between the adjacent microchannels were 600 and 600–800 μm for PJ and SL printing, respectively. Our work highlighted that 3D printing offers a convenient route to design and fabricate 3D microchannels via replica molding, and such 3D microchannels have the potential to tune flows in a manner that would be impossible in planar microchannels. We believe that 3D printing of the molds offers a facile route for the fabrication of 3D microchannels, and the manipulation of flows in 3D microchannels opens up further opportunities for research and applications in microfluidics.

MATERIALS AND METHODS

3D printing of molds

AutoCAD® 2016 (Autodesk, USA) was used to design the molds, and the designs were exported as STL files. Four different printers, one of each for four different 3D printing techniques, were tested.

Fused deposition modeling (FDM)

QiDi Tech 1 FDM printer (Zhejiang QIDI Technology Co., Ltd, Zhejiang, China) was used. The molds were printed using polylactic acid (PLA) filament in 160-μm layers with a 400-μm nozzle. The molds were dry and non-sticky and, therefore, used for subsequent experiments without any further post-processing.

Selective laser sintering (SLS)

Formiga P100 SLS printer (EOS GmbH Electro Optical Systems, Krailling, Germany) was used. The molds were printed using polyamide particles (average grain size 56 μm). The molds were dry and non-sticky and, therefore, used for subsequent experiments without any further post-processing.

Photo-polymer inkjet printing (PJ)

Objet30 Prime PJ printer (Stratasys Ltd, Rehovot, Israel) was used. The molds were printed using the proprietary resin Veroclear in 28 μm layers. The molds were printed in a glossy mode. In the glossy mode, a layer of the support material is first printed, and the part is printed on top of the support layer. After printing, the support material was removed by rinsing thoroughly with water. The washed molds still exhibited a sticky surface. They were soaked in de-ionized (DI) water for 2 h. The molds were subsequently dried with compressed air and placed in an oven at 60 °C for 5 h. This post-processing was carried out to ensure that PDMS does not stick to the molds during the replication.

Stereolithography (SL)

Structo OrthoForm SL printer (Structo Pte. Ltd., Singapore) was used. The molds were printed in 50 μm layers using the proprietary resin from Structo OrthoForm. After printing, the sticky molds were thoroughly cleaned using isopropyl alcohol (IPA). The cleaned molds were placed in a UV chamber for 10 min before subsequent experiments.

Replication of microchannels in PDMS

PDMS base and curing agent (Sylgard 184, silicone elastomer kit, Dow Corning, USA) were thoroughly mixed in a 10 to 1 weight ratio. The mixture was degassed under vacuum until the air bubbles were completely removed. The degassed mixture was poured into 3D-printed molds, and the molds with PDMS were then placed in an oven set at 60 °C for at least 3 h. The molded PDMS replicas were then peeled off gently from the masters. The PDMS replicas were then sealed to glass slides using air plasma treatment (Harrick Plasma PDC 32G).

Metrology

PDMS replica obtained from 3D-printed molds were sectioned across the channels. The sliced cross sections were observed under the microscope (MU500, Amscope, Irvine, CA, USA) to measure the printed width, height, angle, and distance between the channels. Four samples were used to calculate the error bar. The error bars represent the standard deviation. The surface roughness of the molds was measured using a Hirox digital microscope (Hirox, Tokyo, Japan).

Measurement of bonding strength

PDMS channel of $900 \times 900\,\mu m^2$ cross section and a length of 1 cm was sealed to the glass slide via plasma oxidation (Harrick Plasma PDC 32G). A fluid dispenser (Musashi SHOTMASTER®/SHOTmini® ΩX series, Musashi Engineering, Inc., Japan) was used to provide the required pressure. All the devices were tested for 5 s at a given pressure to check for leakage or delamination.

Imaging

Adobe Photoshop was used to enhance all photomicrographs. The photomicrographs were first converted to gray scale, and the brightness and contrast were adjusted. An "Auto Level" function was then employed to further enhance the photomicrographs.

SUPPLEMENTARY MATERIAL

See the supplementary material for more details on (1) 3D-printed molds and (2) commercially available SLS printers.

AUTHORS' CONTRIBUTION

P.P. and S.V. contributed equally to the work. P.P., S.V., and M.H. planned the study. P.P. and S.V. performed the experiments and analyzed the data. P.S.D. and M.H. supervised the research. P.P. and S.V. drafted the manuscript. P.P., S.V., P.S.D., and M.H. edited the manuscript.

ACKNOWLEDGMENTS

P.P. acknowledges the SUTD-MIT postdoctoral fellowship program. S.V. acknowledges the President's Graduate Fellowship awarded by the Ministry of Education (MOE), Singapore. M.H. acknowledges the Start-up Research Grant (No. SREP14088) and Digital Manufacturing and Design (DManD) Center at Singapore University of Technology and Design for allowing us to use equipment (No. RGDM1620403). The authors thank Reno A. L. Leon for help with 3D printing molds using the Structo OrthoForm.

The authors received 3D printed molds from Structo3D for evaluation. The authors declare no competing interests.

DATA AVAILABILITY

The data that support the findings of this study are available within the article and its supplementary material.

REFERENCES

[1]M. G. Roper, "Cellular analysis using microfluidics," Anal. Chem. **88**, 381–394 (2016).
[2]L. Y. Yeo, H. C. Chang, P. P. Chan, and J. R. Friend, "Microfluidic devices for bioapplications," Small **7**, 12–48 (2011).
[3]E. K. Sackmann, A. L. Fulton, and D. J. Beebe, "The present and future role of microfluidics in biomedical research," Nature **507**, 181–189 (2014).
[4]L. Kang, B. G. Chung, R. Langer, and A. Khademhosseini, "Microfluidics for drug discovery and development: From target selection to product lifecycle management," Drug Discov. Today **13**, 1–13 (2008).
[5]R. L. Hartman, J. P. McMullen, and K. F. Jensen, "Deciding whether to go with the flow: Evaluating the merits of flow reactors for synthesis," Angew. Chem. Int. Ed. **50**, 7502–7519 (2011).
[6]A. Abou-Hassan, O. Sandre, and V. Cabuil, "Microfluidics in inorganic chemistry," Angew. Chem. Int. Ed. **49**, 6268–6286 (2010).
[7]D. Liu, H. Zhang, F. Fontana, J. T. Hirvonen, and H. A. Santos, "Microfluidic-assisted fabrication of carriers for controlled drug delivery," Lab Chip **17**, 1856–1883 (2017).
[8]E. W. Young and D. J. Beebe, "Fundamentals of microfluidic cell culture in controlled microenvironments," Chem. Soc. Rev. **39**, 1036–1048 (2010).
[9]Z. Dai, Z. Guo, D. F. Fletcher, and B. S. Haynes, "Taylor flow heat transfer in microchannels—Unification of liquid–liquid and gas–liquid results," Chem. Eng. Sci. **138**, 140–152 (2015).
[10]D. Dendukuri and P. S. Doyle, "The synthesis and assembly of polymeric microparticles using microfluidics," Adv. Mater. **21**, 4071–4086 (2009).
[11]S. E. McCalla and A. Tripathi, "Microfluidic reactors for diagnostics applications," Annu. Rev. Biomed. Eng. **13**, 321–343 (2011).

[12]D. E. Patabadige *et al.*, "Micro total analysis systems: Fundamental advances and applications," Anal. Chem. **88**, 320–338 (2016).
[13]D. C. Duffy, J. C. McDonald, O. J. Schueller, and G. M. Whitesides, "Rapid prototyping of microfluidic systems in poly (dimethylsiloxane)," Anal. Chem. **70**, 4974–4984 (1998).
[14]J. C. McDonald *et al.*, "Fabrication of microfluidic systems in poly (dimethylsiloxane)," Electrophoresis **21**, 27–40 (2000).
[15]K. Ren, J. Zhou, and H. Wu, "Materials for microfluidic chip fabrication," Acc. Chem. Res. **46**, 2396–2406 (2013).
[16]D. Dendukuri, D. C. Pregibon, J. Collins, T. A. Hatton, and P. S. Doyle, "Continuous-flow lithography for high-throughput microparticle synthesis," Nat. Mater. **5**, 365–369 (2006).
[17]M. T. Rahman *et al.*, "Dynamically tunable nanoparticle engineering enabled by short contact-time microfluidic synthesis with a reactive gas," RSC Adv. **3**, 2897 (2013).
[18]M. A. Unger, H.-P. Chou, T. Thorsen, A. Scherer, and S. R. Quake, "Monolithic microfabricated valves and pumps by multilayer soft lithography," Science **288**, 113–116 (2000).
[19]J. A. Weaver, J. Melin, D. Stark, S. R. Quake, and M. A. Horowitz, "Static control logic for microfluidic devices using pressure-gain valves," Nat. Phys. **6**, 218–223 (2010).
[20]N. S. Devaraju and M. A. Unger, "Pressure driven digital logic in PDMS based microfluidic devices fabricated by multilayer soft lithography," Lab Chip **12**, 4809–4815 (2012).
[21]N. Bhattacharjee, C. Parra-Cabrera, Y. T. Kim, A. P. Kuo, and A. Folch, "Desktop-stereolithography 3D-printing of a poly (dimethylsiloxane)-based material with Sylgard-184 properties," Adv. Mater. **30**, 1800001 (2018).
[22]A. Rotem, A. R. Abate, A. S. Utada, V. Van Steijn, and D. A. Weitz, "Drop formation in non-planar microfluidic devices," Lab Chip **12**, 4263–4268 (2012).
[23]M. Hashimoto, R. Langer, and D. S. Kohane, "Benchtop fabrication of microfluidic systems based on curable polymers with improved solvent compatibility," Lab Chip **13**, 252–259 (2013).
[24]J. R. Anderson *et al.*, "Fabrication of topologically complex three-dimensional microfluidic systems in PDMS by rapid prototyping," Anal. Chem. **72**, 3158–3164 (2000).
[25]A. Mata, A. J. Fleischman, and S. Roy, "Fabrication of multi-layer SU-8 microstructures," J. Micromech. Microeng. **16**, 276–284 (2006).
[26]A. D. Stroock *et al.*, "Chaotic mixer for microchannels," Science **295**, 647–651 (2002).
[27]C. Priest, S. Herminghaus, and R. Seemann, "Generation of monodisperse gel emulsions in a microfluidic device," Appl. Phys. Lett. **88**, 024106 (2006).
[28]S. Sugiura, M. Nakajima, S. Iwamoto, and M. Seki, "Interfacial tension driven monodispersed droplet formation from microfabricated channel array," Langmuir **17**, 5562–5566 (2001).
[29]R. Dangla, S. Lee, and C. N. Baroud, "Trapping microfluidic drops in wells of surface energy," Phys. Rev. Lett. **107**, 124501 (2011).
[30]P. Abbyad, R. Dangla, A. Alexandrou, and C. N. Baroud, "Rails and anchors: Guiding and trapping droplet microreactors in two dimensions," Lab Chip **11**, 813–821 (2011).
[31]R. Dangla, S. C. Kayi, and C. N. Baroud, "Droplet microfluidics driven by gradients of confinement," Proc. Natl. Acad. Sci. U.S.A. **110**, 853–858 (2013).
[32]D. Di Carlo, N. Aghdam, and L. P. Lee, "Single-cell enzyme concentrations, kinetics, and inhibition analysis using high-density hydrodynamic cell isolation arrays," Anal. Chem. **78**, 4925–4930 (2006).
[33]A. M. Skelley, O. Kirak, H. Suh, R. Jaenisch, and J. Voldman, "Microfluidic control of cell pairing and fusion," Nat. Methods **6**, 147–152 (2009).
[34]P. Parthiban, P. S. Doyle, and M. Hashimoto, "Self-assembly of droplets in three-dimensional microchannels," Soft Matter **15**, 4244–4254 (2019).
[35]A. Bonyár *et al.*, "3D rapid prototyping technology (RPT) as a powerful tool in microfluidic development," Procedia Eng. **5**, 291–294 (2010).
[36]A. Bonyár *et al.*, "Characterization of rapid PDMS casting technique utilizing molding forms fabricated by 3D rapid prototyping technology (RPT)," J. Mater. Form. **7**, 189–196 (2014).
[37]C. C. Glick *et al.*, "Rapid assembly of multilayer microfluidic structures via 3D-printed transfer molding and bonding," Microsyst. Nanoeng. **2**, 16063 (2016).
[38]G. Comina, A. Suska, and D. Filippini, "PDMS lab-on-a-chip fabrication using 3D printed templates," Lab Chip **14**, 424–430 (2014).
[39]K. Kamei *et al.*, "3D printing of soft lithography mold for rapid production of polydimethylsiloxane-based microfluidic devices for cell stimulation with concentration gradients," Biomed. Microdevices **17**, 36 (2015).
[40]A. Castedo, E. Mendoza, I. Angurell, and J. Llorca, "Silicone microreactors for the photocatalytic generation of hydrogen," Catal. Today **273**, 106–111 (2016).
[41]A. P. Saghati, J. S. Batra, J. Kameoka, and K. Entesari, "A microfluidically reconfigurable dual-band slot antenna with a frequency coverage ratio of 3:1," IEEE Antennas Wirel. Propag. Lett. **15**, 122–125 (2015).
[42]G. L. Coté, M. Robinson, H. Marks, and G. L. Coté, "Comparison of production methods of a spiral inertial microfluidic cell separation device," Proc. SPIE **9715**, 97151C (2016).
[43]J. C. McDonald *et al.*, "Prototyping of microfluidic devices in poly (dimethylsiloxane) using solid-object printing," Anal. Chem. **74**, 1537–1545 (2002).
[44]P. H. King, G. Jones, H. Morgan, M. R. de Planque, and K. P. Zauner, "Interdroplet bilayer arrays in millifluidic droplet traps from 3D-printed moulds," Lab Chip **14**, 722–729 (2014).
[45]A. O. Olanrewaju, A. Robillard, M. Dagher, and D. Juncker, "Autonomous microfluidic capillaric circuits replicated from 3D-printed molds," Lab Chip **16**, 3804–3814 (2016).
[46]A. I. Shallan, P. Smejkal, M. Corban, R. M. Guijt, and M. C. Breadmore, "Cost-effective three-dimensional printing of visibly transparent microchips within minutes," Anal. Chem. **86**, 3124–3130 (2014).
[47]L. Donvito *et al.*, "Experimental validation of a simple, low-cost, T-junction droplet generator fabricated through 3D printing," J. Micromech. Microeng. **25**, 035013 (2015).
[48]J. M. Zhang, E. Q. Li, A. A. Aguirre-Pablo, and S. T. Thoroddsen, "A simple and low-cost fully 3D-printed non-planar emulsion generator," RSC Adv. **6**, 2793–2799 (2016).
[49]S. Vijayan and M. Hashimoto, "3D printed fittings and fluidic modules for customizable droplet generators," RSC Adv. **9**, 2822–2828 (2019).
[50]Q. Ji *et al.*, "A modular microfluidic device via multimaterial 3D printing for emulsion generation," Sci. Rep. **8**, 1–11 (2018).
[51]Y. Morimoto, M. Kiyosawa, and S. Takeuchi, "Three-dimensional printed microfluidic modules for design changeable coaxial microfluidic devices," Sens. Actuators B Chem. **274**, 491–500 (2018).
[52]T. Ching, Y.-C. Toh, and M. Hashimoto, "Fabrication of complex 3D fluidic networks via modularized stereolithography," Adv. Eng. Mater. **22**, 1901109 (2020).
[53]T. Ching *et al.*, "Fabrication of integrated microfluidic devices by direct ink writing (DIW) 3D printing," Sens. Actuators B Chem. **297**, 126609 (2019).
[54]T. Femmer *et al.*, "High-throughput generation of emulsions and microgels in parallelized microfluidic drop-makers prepared by rapid prototyping," ACS Appl. Mater. Interfaces **7**, 12635–12638 (2015).
[55]R. Walczak and K. Adamski, "Inkjet 3D printing of microfluidic structures—On the selection of the printer towards printing your own microfluidic chips," J. Micromech. Microeng. **25**, 085013 (2015).
[56]J. M. Lee, M. Zhang, and W. Y. Yeong, "Characterization and evaluation of 3D printed microfluidic chip for cell processing," Microfluid. Nanofluid. **20**, 5 (2016).
[57]A. K. Au, W. Lee, and A. Folch, "Mail-order microfluidics: Evaluation of stereolithography for the production of microfluidic devices," Lab Chip **14**, 1294–1301 (2014).
[58]N. P. Macdonald *et al.*, "Comparing microfluidic performance of three-dimensional (3D) printing platforms," Anal. Chem. **89**, 3858–3866 (2017).
[59]N. Mohd Fuad, M. Carve, J. Kaslin, and D. Wlodkowic, "Characterization of 3D-printed moulds for soft lithography of millifluidic devices," Micromachines **9**, 116 (2018).

[60]T. Brajlih, B. Valentan, J. Balic, and I. Drstvensek, "Speed and accuracy evaluation of additive manufacturing machines," Rapid Prototyp. J. **17**, 64–75 (2011).
[61]M. C. Yuen and R. K. Kramer, in *2016 International Manufacturing Science and Engineering Conference* (American Society of Mechanical Engineers, 2016).
[62]O. D. Yirmibesoglu *et al.*, in *2018 IEEE International Conference on Soft Robotics (RoboSoft)* (IEEE, 2018), pp. 295–302.
[63]H. N. Chan *et al.*, "Direct, one-step molding of 3D-printed structures for convenient fabrication of truly 3D PDMS microfluidic chips," Microfluid. Nanofluid. **19**, 9–18 (2015).
[64]A. K. Au, W. Huynh, L. F. Horowitz, and A. Folch, "3D-printed microfluidics," Angew. Chem. Int. Ed. **55**, 3862–3881 (2016).
[65]A. Mazzoli, "Selective laser sintering in biomedical engineering," Med. Biol. Eng. Comput. **51**, 245–256 (2013).
[66]J.-P. Kruth, G. Levy, F. Klocke, and T. Childs, "Consolidation phenomena in laser and powder-bed based layered manufacturing," CIRP Ann. **56**, 730–759 (2007).
[67]See https://www.3dhubs.com/knowledge-base/post-processing-sls-printed-parts/#standard for post-processing of SL-printed models.
[68]J. C. Brooks, K. I. Ford, D. H. Holder, M. D. Holtan, and C. J. Easley, "Macro-to-micro interfacing to microfluidic channels using 3D-printed templates: Application to time-resolved secretion sampling of endocrine tissue," Analyst **141**, 5714–5721 (2016).
[69]N. Jayanth, P. Senthil, and C. Prakash, "Effect of chemical treatment on tensile strength and surface roughness of 3D-printed ABS using the FDM process," Virtual Phys. Prototyping **13**, 155–163 (2018).
[70]L. M. Galantucci, F. Lavecchia, and G. Percoco, "Experimental study aiming to enhance the surface finish of fused deposition modeled parts," CIRP Ann. **58**, 189–192 (2009).
[71]T. K. Nguyen and B.-K. Lee, "Post-processing of FDM parts to improve surface and thermal properties," Rapid Prototyp. J. **24**, 1091–1100 (2018).
[72]C.-S. Park, K.-I. Joo, S.-W. Kang, and H.-R. Kim, "A PDMS-coated optical fiber Bragg grating sensor for enhancing temperature sensitivity," J. Opt. Soc. Korea **15**, 329–334 (2011).
[73]C. Li *et al.*, "A review of coating materials used to improve the performance of optical fiber sensors," Sensors **20**, 4215 (2020).
[74]Y. Hwang, O. H. Paydar, and R. N. Candler, "3D printed molds for non-planar PDMS microfluidic channels," Sens. Actuator A Phys. **226**, 137–142 (2015).
[75]M. P. Lee *et al.*, "Development of a 3D printer using scanning projection stereolithography," Sci. Rep. **5**, 9875 (2015).
[76]Z. Wang, N. Martin, D. Hini, B. Mills, and K. Kim, "Rapid fabrication of multilayer microfluidic devices using the liquid crystal display-based stereolithography 3D printing system," 3D Print Addit. Manuf. **4**, 156–164 (2017).
[77]S. Knowlton *et al.*, "3D-printed microfluidic chips with patterned, cell-laden hydrogel constructs," Biofabrication **8**, 025019 (2016).
[78]M. Mao *et al.*, "The emerging frontiers and applications of high-resolution 3D printing," Micromachines **8**, 113 (2017).
[79]H. Gong, B. P. Bickham, A. T. Woolley, and G. P. Nordin, "Custom 3D printer and resin for 18 μm × 20 μm microfluidic flow channels," Lab Chip **17**, 2899–2909 (2017).